Cell Reports

Report

A Regulatory Switch Alters Chromosome Motions at the Metaphase-to-Anaphase Transition

Graphical Abstract

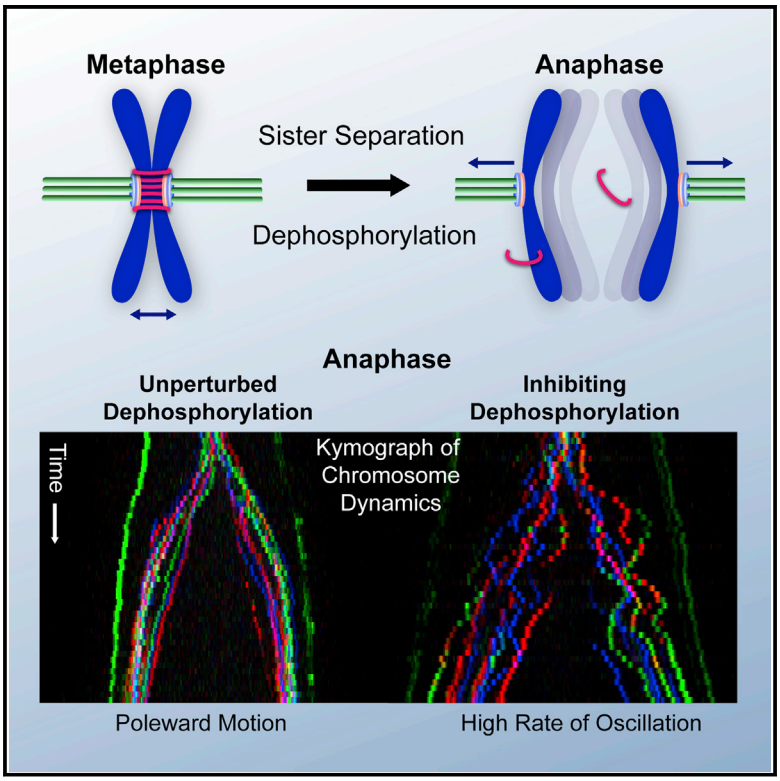

Highlights

- A live-imaging assay was used to track anaphase chromosome motion in human cells
- Sister chromatid separation is insufficient to induce anaphase chromosome behavior
- Global dephosphorylation controls anaphase chromosome motion
- Chromokinesin and kinetochore-derived forces promote chromosome oscillations

Authors

Kuan-Chung Su, Zachary Barry, Nina Schweizer, Helder Maiato, Mark Bathe, Iain McPherson Cheeseman

Correspondence

icheese@wi.mit.edu

In Brief

Su et al. perform tracking analysis of chromosome motion in anaphase human cells. They find that changes in global phosphorylation are crucial for normal anaphase chromosome dynamics. Inhibiting dephosphorylation induces anti-polar motion of chromosomes in anaphase. The authors also identify molecular players that contribute to these chromosome movements.

Su et al., 2016, Cell Reports *17*, 1–11
November 8, 2016
http://dx.doi.org/10.1016/j.celrep.2016.10.046

CellPress

Please cite this article in press as: Su et al., A Regulatory Switch Alters Chromosome Motions at the Metaphase-to-Anaphase Transition, Cell Reports (2016), http://dx.doi.org/10.1016/j.celrep.2016.10.046

Cell Reports
Report

A Regulatory Switch Alters Chromosome Motions at the Metaphase-to-Anaphase Transition

Kuan-Chung Su,[1] Zachary Barry,[3] Nina Schweizer,[4,5] Helder Maiato,[4,5,6] Mark Bathe,[3] and Iain McPherson Cheeseman[1,2,7,*]
[1]Whitehead Institute for Biomedical Research, Nine Cambridge Center, Cambridge, MA 02142, USA
[2]Department of Biology, Massachusetts Institute of Technology, Cambridge, MA 02142, USA
[3]Department of Biological Engineering, Massachusetts Institute of Technology, Cambridge, MA 02139, USA
[4]Chromosome Instability and Dynamics Laboratory, Instituto de Biologia Molecular e Celular, Universidade do Porto, 4200-135 Porto, Portugal
[5]i3S – Instituto de Inovação e Investigação em Saúde, Universidade do Porto, 4200-135 Porto, Portugal
[6]Cell Division Unit, Department of Experimental Biology, Faculdade de Medicina, Universidade do Porto, 4200-135 Porto, Portugal
[7]Lead Contact
*Correspondence: icheese@wi.mit.edu
http://dx.doi.org/10.1016/j.celrep.2016.10.046

SUMMARY

To achieve chromosome segregation during mitosis, sister chromatids must undergo a dramatic change in their behavior to switch from balanced oscillations at the metaphase plate to directed poleward motion during anaphase. However, the factors that alter chromosome behavior at the metaphase-to-anaphase transition remain incompletely understood. Here, we perform time-lapse imaging to analyze anaphase chromosome dynamics in human cells. Using multiple directed biochemical, genetic, and physical perturbations, our results demonstrate that differences in the global phosphorylation states between metaphase and anaphase are the major determinant of chromosome motion dynamics. Indeed, causing a mitotic phosphorylation state to persist into anaphase produces dramatic metaphase-like oscillations. These induced oscillations depend on both kinetochore-derived and polar ejection forces that oppose poleward motion. Thus, our analysis of anaphase chromosome motion reveals that dephosphorylation of multiple mitotic substrates is required to suppress metaphase chromosome oscillatory motions and achieve directed poleward motion for successful chromosome segregation.

INTRODUCTION

During mitosis in vertebrate cells, several sequential phases occur to distribute replicated sister chromatids to daughter cells. First, during prometaphase, chromosomes form attachments to spindle microtubules and are moved to the center of the cell in a process termed congression. At metaphase, chromosomes align at the metaphase plate where they undergo oscillations (Jaqaman et al., 2010; Skibbens et al., 1993). Finally, during anaphase, sister chromatids are separated and segregated toward opposite spindle poles (Maiato and Lince-Faria, 2010).

Chromosome congression and metaphase chromosome oscillations have been the subject of intense investigation (reviewed in Vladimirou et al., 2011). These studies have revealed that multiple factors acting on chromosomes are integrated to achieve the observed chromosome motion. This includes the attachment of kinetochores to microtubules, changes in microtubule dynamics that act to push or pull on kinetochores (Dumont et al., 2012; Inoué and Salmon, 1995), chromosome cohesion between replicated sister chromatids that provides a spring-like connection between them, and chromokinesin-dependent polar ejection forces (Civelekoglu-Scholey et al., 2013; Joglekar and Hunt, 2002).

Despite extensive work on metaphase chromosome dynamics, the nature and molecular origin of anaphase chromosome motion are less well understood. Here, we established a procedure to image the metaphase-to-anaphase transition and anaphase chromosome motion, with high temporal resolution in human cells, to assess the dynamics of anaphase chromosome motion and the mechanisms that direct sister chromatid segregation. Our results indicate that changes in chromosome motion at anaphase onset do not result from the physical separation of sister chromatids. Instead, we find that poleward chromosome motion in anaphase requires critical changes to the global phosphorylation state of the cell. Our results suggest that a change in the phosphorylation state of factors required for kinetochore-derived forces and chromokinesin-dependent polar ejection forces provides a regulatory switch to alter chromosome motion between metaphase and anaphase. Thus, the regulatory changes that occur at anaphase onset and the precise timing of sister chromatid separation act together to ensure the proper segregation of sister chromatids to daughter cells.

RESULTS

Tracking Analysis of Anaphase Chromosome Motion

To analyze the behavior of anaphase chromosome motion in human cells, we generated human cancer (HeLa) and

Please cite this article in press as: Su et al., A Regulatory Switch Alters Chromosome Motions at the Metaphase-to-Anaphase Transition, Cell Reports (2016), http://dx.doi.org/10.1016/j.celrep.2016.10.046

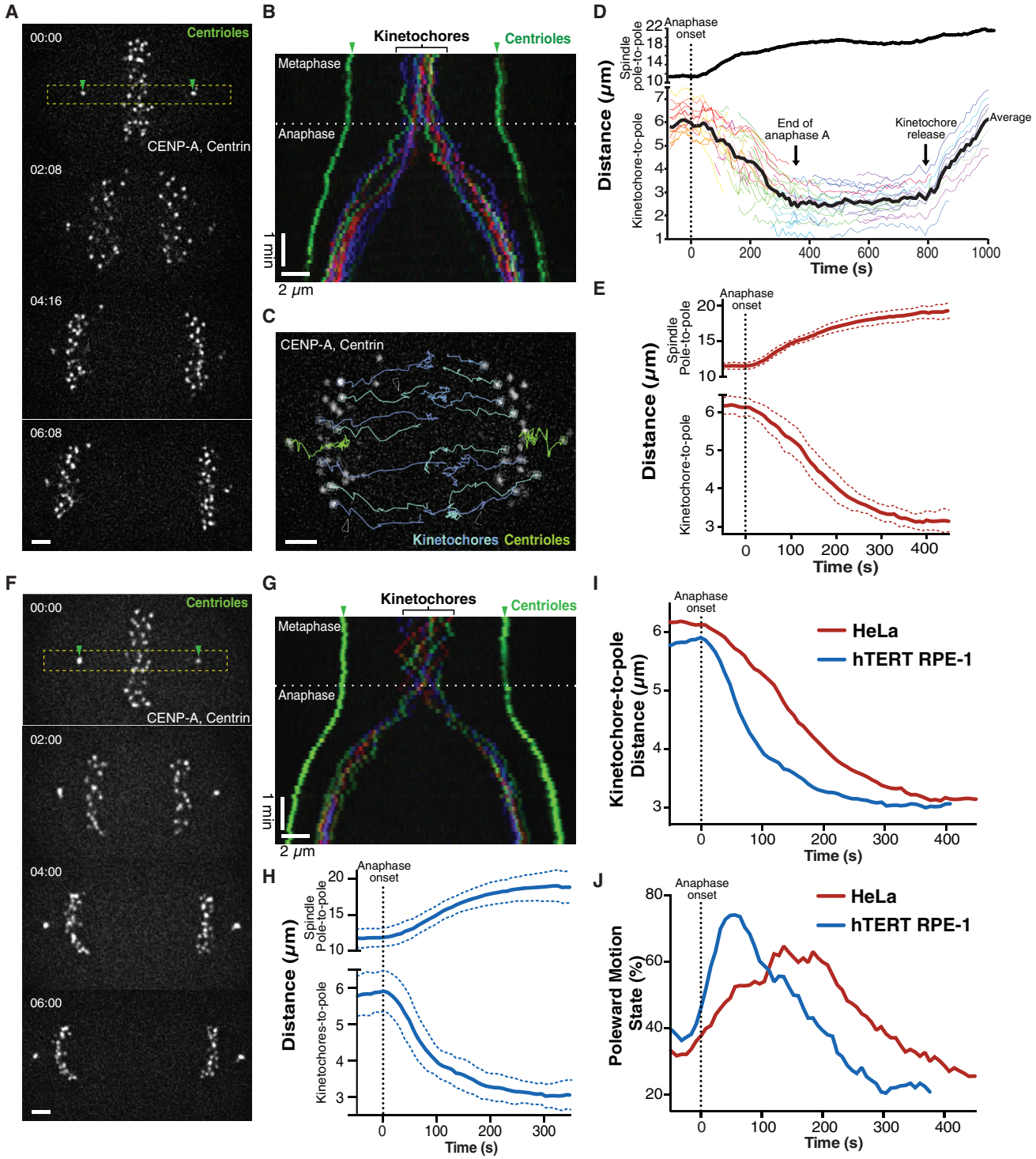

Figure 1. Analysis of Anaphase Chromosome Dynamics in Human Cells

(A) Still images from a time-lapse movie of HeLa cells expressing 3×GFP-CENP-A, 3×GFP-centrin. Box indicates the section used to generate the kymograph.

(B) Color-coded kymograph of the time-lapse movie from (A) is shown.

(C) Representative image of time-lapse series displayed in (A) is overlaid with selected tracks of particles.

(D) Graph showing the distances over time for the distance between spindle poles (top; to measure spindle elongation) and the kinetochore-to-pole distance (bottom; to visualize chromosome motion) using tracks of an HeLa cell. The average kinetochore-to-pole distance is indicated as a black line, with individual kinetochores indicated in color. The time of anaphase onset is indicated by the dashed line.

(legend continued on next page)

non-transformed (hTERT RPE-1) cell lines stably expressing the centromere protein CENP-A and the centriole component Centrin (CETN1), each fused to 3× tandem repeats of GFP. We performed live-cell imaging of these cells progressing through mitosis (Figure 1) to visualize the trajectories of individual kinetochores and their motion relative to the spindle pole (Figure 1D; Figure S1A). Using single-particle tracking and trajectory analysis, we were able to assess anaphase chromosome segregation to distinguish the anaphase A-based motion of kinetochores toward the spindle poles (Figures 1D, 1E, and 1H, lower graphs) and the anaphase B-based separation of the spindle poles (Figures 1D, 1E, and 1H, upper graphs; Table S1) in a model-free manner (Monnier et al., 2015). We found that the overall dynamics of spindle pole separation and chromosome motion were similar in HeLa and hTERT RPE-1 cells (see Table S1).

Prior work in other organisms has found that the forces acting on bi-oriented sister chromatids prevent spindle elongation until the sister chromatids are separated at anaphase onset (Desai et al., 2003). Consistent with this, we observed that spindle elongation initiated coincident with visually discernible sister chromatid separation in both HeLa and hTERT RPE-1 cells (Figures 1D, 1E, and 1H). We predicted that the loss of a physical connection between sisters at anaphase onset also would induce the rapid motion of chromatids toward their associated poles. However, although hTERT RPE-1 cells displayed a rapid increase in overall poleward motion shortly following anaphase onset, HeLa cells showed a delay of ~80 s in achieving a maximal rate of average poleward motion (Figure 1I). Once chromosomes reached a distance of ~3 μm from the spindle pole, they maintained this position as the spindle poles continued to elongate (Figures 1D, 1E, and 1H). At the end of anaphase, the kinetochore-to-pole distance increased suddenly and synchronously (Figure 1D; Figure S1B), indicating the release of the kinetochores from the spindle poles by eliminating kinetochore-microtubule interactions. This provides an assay to systematically analyze anaphase chromosome motion in human cells.

Disrupting the Opposing Forces Acting on Sister Chromatids Is Insufficient to Explain the Suppression of Chromosome Oscillations at Anaphase Onset

The metaphase-to-anaphase transition is characterized by a switch between metaphase chromosome oscillations and directional anaphase poleward motion. To analyze this switch in behavior, we classified distinct periods of kinetochore motion as either poleward or anti-poleward (see the Supplemental Experimental Procedures and Figure S1F). In cases where a kinetochore moved less than the experimentally determined localization error (see Figures S1C and S1D) between successive time points, it was classified as having indeterminate motion during this corresponding time interval.

During metaphase, HeLa cells displayed an equivalent fraction of poleward and anti-poleward motion, with 33% ± 2% (mean ± SD; mean was measured as cell-to-cell variation after averaging kinetochore motion in individual cells; see the Supplemental Experimental Procedures for additional information) poleward events and 33% ± 3% anti-poleward events (Table S2). In contrast, during the early phase following anaphase onset (240 s in HeLa and 152 s in hTERT RPE-1), we observed both poleward and anti-poleward motions, but the majority of kinetochore motion was poleward, as expected for anaphase A sister chromatid segregation (Figure 1J; Table S1). For example, kinetochores in HeLa cells moved poleward for 54% ± 2% of events detected during early anaphase, with only 20% ± 3% of their motion spent in the anti-poleward state. However, in comparison with hTERT RPE-1 cells, HeLa cells were delayed in achieving a maximal proportion of poleward motion (Figure 1J; Table S1).

To determine the molecular origin of the transition from clearly distinct chromosome motions in metaphase versus anaphase, we first considered the physical connections that differ between these two phases. At anaphase onset, physical associations between sister chromatids are eliminated by the cleavage of cohesin molecules (Hauf et al., 2001). To disrupt sister chromatid cohesion prematurely in our human cell culture system, we depleted the cohesin complex subunit Rad21 by RNAi (Figure 2A). Rad21-depleted cells displayed separated sister chromatids that failed to congress to the metaphase plate, but these chromatids continued to exhibit both poleward (33% ± 5%) and anti-poleward (44% ± 8%) motions (Figure 2A; Figure S2A), consistent with prior studies using tobacco etch virus (TEV) protease-induced cohesion cleavage in *Drosophila* embryos (Oliveira et al., 2010). We also used laser ablation to eliminate a single kinetochore from a pair of sister chromatids in a metaphase cell, thereby removing the pulling forces created by the connection to the opposing spindle pole (Figure 2B). In these laser ablation experiments, the released kinetochore initially moved away from the metaphase plate during the first 20 s after ablation, displaying net poleward motion (69% ± 25% poleward motion and 13% ± 18% anti-poleward motion). However, these released kinetochores then displayed a balance of poleward (40% ± 8%) and anti-poleward (35% ± 10%) motions (Figure S2A) that resembled the behavior of bi-oriented metaphase chromosomes (Figure 2B; Figure S2B; Table S2; also see Rieder et al., 1986; Skibbens et al., 1995).

Reciprocally, to cause connections between sister chromatids to persist into anaphase, we treated cells with the topoisomerase II inhibitor ICRF193, which prevents the resolution of ultrafine DNA bridges (UFBs; Wang et al., 2008). UFBs are generated between sister chromatids during DNA replication, but they are resolved in metaphase and early anaphase (Liu et al., 2014). Treatment with 1 μM ICRF193 significantly delayed UFB

(E) Average spindle pole-to-pole distance (upper graph) and kinetochore-to-pole distance (lower graph) for HeLa cells undergoing anaphase (n = 10). Colored dotted lines indicate SD between cells.
(F–H) Still images from a time-lapse movie of an hTERT RPE-1 cell expressing 3×GFP-CENP-A, 3×GFP-centrin. (G) Color-coded kymograph of time-lapse movie still displayed in (F). (H) Average spindle pole-to-pole distance (upper graph) and kinetochore-to-pole distance (lower graph) of hTERT RPE-1 cell undergoing anaphase is shown (n = 10). Blue dotted lines indicate SD between cells.
(I) Direct comparison of average kinetochore-to-pole distances over time for HeLa (from E) and hTERT-RPE cell data (from H) is shown.
(J) Percentage of poleward motion over time is shown. Scale bars, 2 μm. See also Figure S1, Tables S1 and S2, and Movie S1.

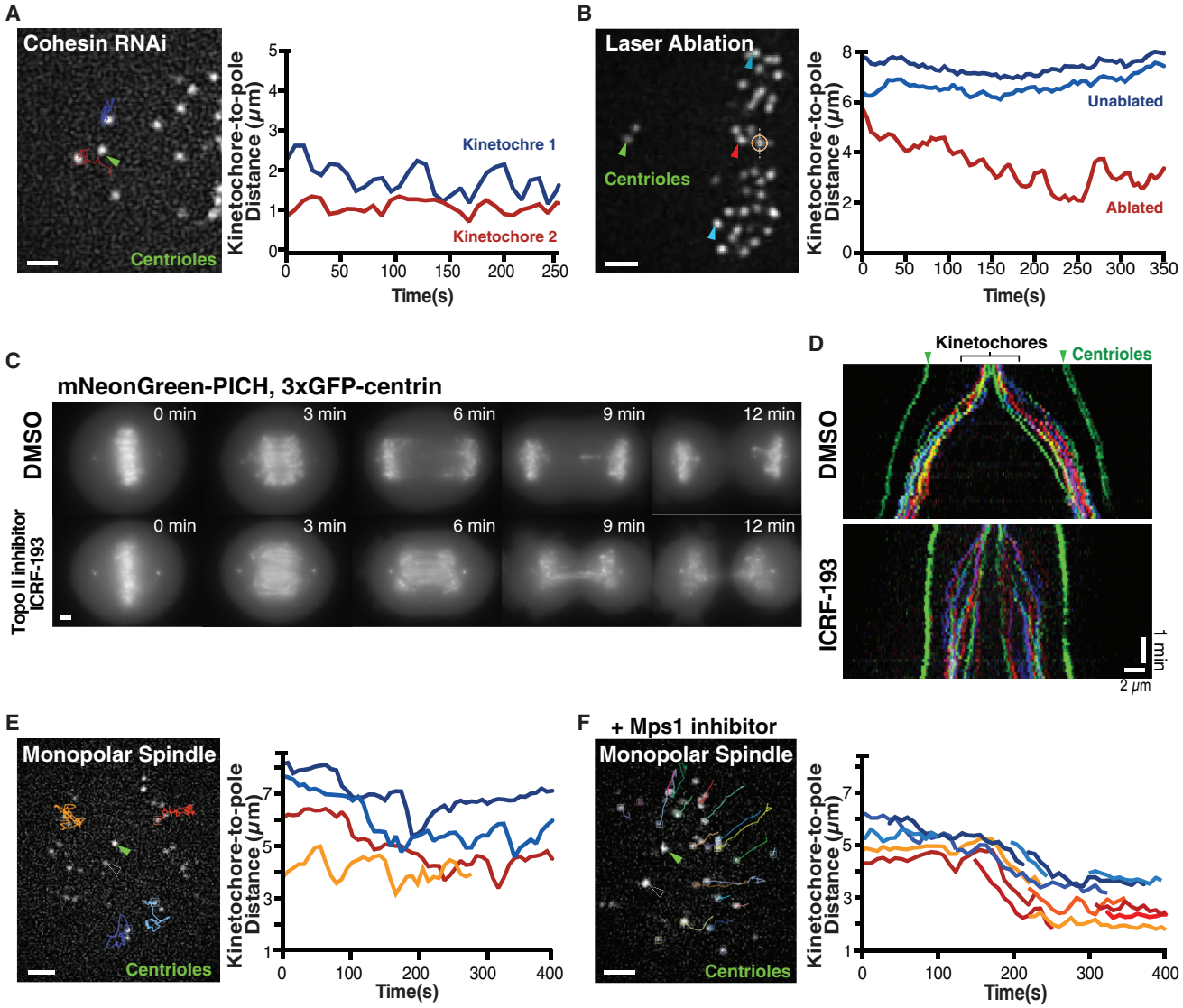

Figure 2. Physical Connections between Sister Chromatids Are Not Required for Anti-poleward Motion

(A) Still image from a representative time-lapse movie shows an HeLa cell (3×GFP-CENP-A, 3×GFP-centrin; n = 20) following depletion of the cohesin subunit RAD21 (48 hr), displaying tracks until current time point of selected kinetochores used to generate the kinetochore-to-spindle pole distance graph (right).

(B) Image of an HeLa cell (3×GFP-CENP-A, 3×GFP-centrin) before laser ablation (orange hair cross) to inactivate one of two sister kinetochores (n = 29 experiments). Arrowhead indicates the released kinetochore (red) or unaffected kinetochores (blue), which were tracked to generate spindle-to-pole distance graph (right).

(C) Maximal intensity projections of still images from representative time-lapse sequences show HeLa cells expressing mNeonGreen-PICH, 3×GFP-centrin, entering anaphase in the presence of DMSO (n = 10) or 1 μM of the topoisomerase inhibitor ICRF-133 (n = 14).

(D) Color-coded kymographs show HeLa cells (3×GFP-CENP-A, 3×GFP-centrin) from anaphase onward treated with DMSO (n = 5) or ICRF-193 (n = 7).

(E) Still image from a time-lapse movie of an HeLa cell (3×GFP-CENP-A, 3×GFP-centrin), treated with S-trityl-L-cysteine (STLC) to generate a monopolar spindle (n = 11), shows tracks of the selected kinetochores used to generate kinetochore-to-spindle pole distance graph (right).

(F) Image from a time-lapse movie of a monopolar HeLa cell (3×GFP-CENP-A, 3×GFP-centrin) treated with STLC and the Mps1 inhibitor AZ3146 (n = 8). Selected tracks were used to generate the kinetochore-to-spindle pole distance graph (right). Green arrowheads highlight spindle poles; t = 0 is the beginning of the movie. Scale bars, 2 μm. See also Figure S2, Table S2, and Movie S2.

resolution, as detected by the presence of the UFB marker mNeonGreen-PICH (Chan et al., 2007), resulting in decreased spindle elongation (Figures 2C and 2D). However, in cells treated with ICRF193, the majority of the kinetochores moved toward the spindle poles, and we did not detect a noticeable increase in anti-poleward motion (Figure 2D). We note that UFBs do retard the rate of chromosome movement, possibly by acting to provide resistance similar to that created by sister chromatid cohesion. In summary, although a physical connection between sister chromatids controls the amplitude and period of metaphase

chromosome oscillations (Burroughs et al., 2015; Wan et al., 2012), removing these connections is not sufficient to induce the change in the proportion of poleward and anti-poleward motions that occurs at anaphase onset.

Preventing Protein Dephosphorylation Induces Dramatic Chromosome Oscillations in Anaphase

We next considered whether changes to the cell regulatory environment are responsible for the altered chromosome dynamics at anaphase onset. To test the relative contributions of the forces acting on the sister chromatid and the cell regulatory state, we generated monopolar spindles using S-trityl-L-cysteine (STLC) to inhibit the kinesin-5 motor Eg5, which causes all poleward-pulling forces to emanate from a single origin. Despite the absence of bi-oriented attachments in STLC-treated cells, we observed both poleward and anti-poleward motions (Figure 2E). However, triggering anaphase onset by inactivating the spindle assembly checkpoint using an Mps1 inhibitor was sufficient to induce a synchronous directional motion toward the single pole (Figure 2F; also see Canman et al., 2003).

Protein dephosphorylation is a hallmark of mitotic exit (Wurzenberger and Gerlich, 2011), and it alters microtubule dynamics required for chromosome segregation (Higuchi and Uhlmann, 2005). To inhibit protein dephosphorylation, we treated metaphase HeLa cells with 1 μM Okadaic acid, a potent inhibitor of both PP1 and PP2A phosphatases. Okadaic acid treatment resulted in dramatic metaphase-like chromosome oscillations that persisted into anaphase (Figures 3A and 3B). These oscillations reflect a statistically significant increase in the proportion of anti-poleward motion (30% ± 5%; Figure 3C; Table S2), with a similar proportion of anti-poleward-moving kinetochores to that observed in metaphase cells (33% ± 3%; Figure 3D; Figure S3A). The change in chromosome movement was not due to the persistence of UFBs based on mNeonGreen-PICH fluorescence (Figure S3B). In addition to altering the proportion of poleward/anti-poleward motions, Okadaic acid treatment significantly increased the velocity of both poleward- and anti-poleward-moving kinetochores (Figure 3C; Figures S3C and S3D; Table S2). Interestingly, this rate was higher than that observed for metaphase kinetochores (Figure S3D; Table S2), likely due to opposing forces, derived from the attached sister kinetochore in metaphase, that act to retard chromosome motion.

We also observed a similar effect following treatment with the phosphatase inhibitor cantharidic acid (data not shown). This effect was considerably more severe than that observed in prior work that inhibited a subset of PP1 function by the depletion of Sds22 or Repo-man, which induced occasional pausing and infrequent anti-polar motion in anaphase (Wurzenberger et al., 2012). Previous work expressing high levels of a non-degradable version of cyclin B, to prevent the downregulation of CDK1 activity, found that this prevented normal anaphase progression after sister chromatid separation, resulting in a metaphase-like arrest (Vázquez-Novelle et al., 2014). We found that expression of lower levels of non-degradable cyclin B permitted full progression into anaphase and cytokinesis but resulted in dramatic anaphase chromatid oscillations (Figure 3E), similar to Okadaic acid treatment (Figure 3A). Therefore, dephosphorylation of target proteins downstream of CDK1 by PP1 and PP2A is essential for the changes in chromosome dynamics that occur at anaphase onset. Allowing a metaphase phosphorylation state to persist into anaphase results in dramatic metaphase-like chromosome oscillations, despite the separation of sister chromatids.

Both Chromosome and Kinetochore-Derived Forces Contribute to Anaphase Anti-poleward Motion in Okadaic Acid-Treated Cells

We next sought to determine the origin of the induced chromosome oscillations that occur during anaphase when protein dephosphorylation is perturbed. To assess the sources of the force acting on the sister chromatids, we first tested whether Okadaic acid-induced anti-poleward motion requires polar ejection forces. The chromokinesins KID and KIF4A act on the chromosome arms during metaphase to push chromosomes away from the spindle poles, and, thereby, they contribute to metaphase chromosome oscillations (Antonio et al., 2000; Funabiki and Murray, 2000; Levesque and Compton, 2001; Wandke et al., 2012).

To test the role of polar ejection forces during anaphase, we generated CRISPR/Cas9-mediated knockout cell lines for the chromokinesins *KID* and *KIF4A* (Figure S4A). Individual elimination of KID or KIF4A resulted in a reduced distance between kinetochores and the spindle poles in cells with monopolar spindles, consistent with a role for these motors in generating polar ejection force. The *KID* + *KIF4A* double-knockout cell line displayed an enhanced reduction in the kinetochore-spindle pole distance (Figure S4B), consistent with previous RNAi-based experiments (Barisic et al., 2014; Wandke et al., 2012). However, despite this strong effect on chromosome-pole distances during mitosis, the *KID* + *KI4A* double-knockout cell line was viable (Figure S4A).

We next assessed whether polar ejection forces act during an unperturbed anaphase. As described above, control cells display a plateau in poleward motion during anaphase A such that they halt their next poleward motion when they reach a distance of ~3 μm away from the spindle pole. In contrast, we found that the *KID* + *KIF4A* double-knockout cell line displayed a reduced kinetochore-to-pole distance at the end of anaphase A (Figure S4C). This suggests that the activity of these chromokinesins persists into anaphase, where they contribute to the plateau in poleward motion (Figure 1D). However, *KID* + *KIF4A* double-knockout cells did not otherwise display a striking difference in anaphase chromosome dynamics in untreated cells. Interestingly, we found that the proportion of anti-poleward motion in anaphase was modestly but statistically significantly decreased in the *KID* + *KIF4A* double knockout in Okadaic acid-treated cells (Figures 4A and 4B; Table S2). Thus, chromokinesin-based polar ejection forces contribute to the Okadaic acid-induced, anti-poleward anaphase motions.

We next tested the contributions of the kinetochore-associated motor Kif18A, which acts to dampen the chromosome dynamics in metaphase (Du et al., 2010; Stumpff et al., 2008, 2012). HeLa cells depleted of Kif18A by RNAi displayed increased metaphase chromosome oscillations (Figure S4D), defects in chromosome congression, and a delay in the mitotic progression (Figure S4E). Using the Mps1 inhibitor AZ3146 to control the timing of anaphase onset in Kif18A-depleted cells

Please cite this article in press as: Su et al., A Regulatory Switch Alters Chromosome Motions at the Metaphase-to-Anaphase Transition, Cell Reports (2016), http://dx.doi.org/10.1016/j.celrep.2016.10.046

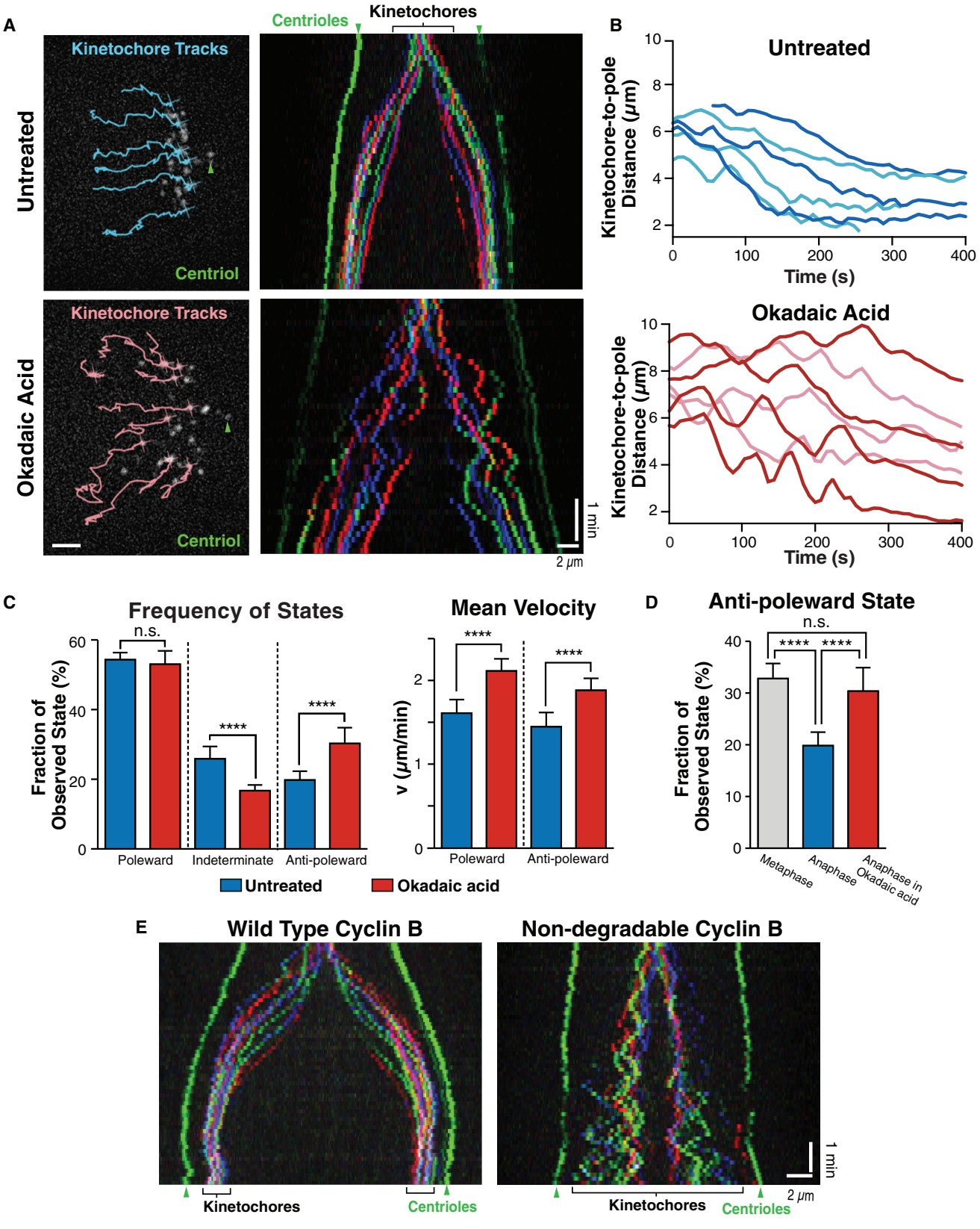

(legend on next page)

treated with 1 μM Okadaic acid, we observed a further increase of anaphase chromatid oscillations (Figures 4C and 4D; Table S2), similar to the enhanced metaphase oscillations that occur in Kif18A-depleted cells (Stumpff et al., 2008).

Finally, to test whether kinetochore-derived forces contribute to the observed anaphase motion, we used a mutant of the kinetochore protein Ska1 complex, which we previously have shown inhibits chromosome oscillations during metaphase (Schmidt et al., 2012). We generated stable cell lines expressing mCherry fused to RNAi-resistant versions of wild-type Ska1 or a mutant of Ska1 lacking the microtubule-binding domain (ΔMTBD). In cells in which Ska1 was replaced with the Ska1ΔMTBD mutant, we did not detect a significant change in chromosome dynamics during anaphase in untreated cells (Figure S4F). Strikingly, we observed a complete loss of the Okadaic-induced oscillations during anaphase in Ska1ΔMTBD mutant cells (Figures 4E and 4F). We observed a significant decrease in the fraction of anti-poleward motions and the rate of both polar and anti-poleward motions, such that these were similar to anaphase cells in the absence of Okadaic acid (Figures 4E–4H; Table S2). Together, these analyses indicate that both chromosome and kinetochore-derived forces are required for the Okadaic acid-induced chromosome oscillations during anaphase.

DISCUSSION

A Phospho-Regulatory Switch Regulates Anaphase Chromosome Dynamics

By analyzing the dynamics of chromosome movements under diverse conditions, including physical, pharmacological, and genetic perturbations, our work demonstrates that the movement behavior of mitotic chromosomes in human cells is determined primarily by the cellular regulatory environment (Figure 5). The physical connections between sister chromatids contribute to controlling the period and amplitude of sister chromatid oscillations during mitosis, but they do not control the proportion of poleward and anti-poleward motions. Indeed, in prometaphase, the premature removal of cohesin or the loss of a connection to one of the spindle poles does not preclude anti-poleward and oscillatory motions (Figures 2A and 2B), similar to prior observations in *Drosophila* embryos (Oliveira et al., 2010; Parry et al., 2003). Reciprocally, causing a metaphase regulatory state to persist into anaphase using phosphatase inhibition or non-degradable cyclin B expression dramatically increases anti-poleward motion (Figures 3A and 3E; Table S2).

We found that the anti-poleward motion requires proteins that have been implicated in metaphase oscillations, including factors that contribute to kinetochore-derived forces and polar ejection forces. An overall change in the microtubule turnover takes place at the metaphase-to-anaphase transition (Zhai et al., 1995). Consistent with this, previous work found that Kif18A (Häfner et al., 2014), which acts to dampen microtubule dynamics, and the chromokinesin KID (Ohsugi et al., 2003) are regulated downstream of CDK. A change in their phosphorylation status at anaphase onset may act to dampen chromosome oscillations and reduce polar ejection forces. Similarly, kinetochore-derived forces that depend on the Ska1 complex also must be altered upon mitotic exit to suppress the persistence of oscillations into anaphase. Thus, a broad spectrum of targets is regulated directly and indirectly downstream of CDK, and their combined action alters the dynamics of microtubules and chromosome motion. In summary, our work reveals that the switch of chromosome motion from metaphase to anaphase is not simply the result of a physical separation of sister chromatids but additionally requires changes in the phosphorylation of multiple mitotic targets that collectively regulate chromosome poleward motion. This may ensure that chromosome segregation is precisely coordinated with other phosphorylation-regulated steps of mitotic exit, such as furrow ingression or nuclear membrane reformation, to ensure proper genome separation and integrity.

EXPERIMENTAL PROCEDURES

Cell Culture and Cell Line Generation

HeLa and hTERT RPE-1 cells were maintained under standard tissue conditions (Schmidt et al., 2012). Cells expressing fluorescent tag fusions of Centrin (CETN1), CENP-A, PICH, Ska1 wild-type, or ΔMTBD (Schmidt et al., 2012) were generated using retroviral infection of cells with pBABE-based vectors, as previously described (Cheeseman et al., 2004). CRISPR/Cas9-mediated knockout cells were generated by co-transfection of px330 (Cong et al., 2013) targeting *KID* (GCAGAGGCGACGCGAGATGG) or *KIF4A* (GCTCTCCGG GCACGAAGGAA) with CS2 + mCherry (1:10) using FuGENE HD (Promega), according to the manufacturer's instructions, and sorting for single cells using mCherry signal after 2 days. Clones were verified via western blotting using antibodies (Abcam) against KID (1:1,000, ab69824) or KIF4A (1:2,000, ab124903) and α-tubulin (1:2,000, ab40742). For a list of cell lines used in this study, see the Supplemental Experimental Procedures.

Drug Treatment and Cell Transfection

Where indicated, cells were incubated in 1 μM ICRF193 (Santa Cruz Biotechnology), 1 μM Okadaic acid (Santa Cruz Biotechnology), or 2 μM AZ3146

Figure 3. Perturbing the Cellular Phosphorylation State Induces Anaphase Anti-poleward Chromosome Motion

(A) (Left) Images of untreated HeLa cells (3×GFP-CENP-A, 3×GFP-centrin) or cells treated with Okadaic acid ($n \geq 10$ cells). Selected kinetochore tracks until current time point are displayed. (Right) Color-coded kymographs from the corresponding movies starting at anaphase onset are shown.

(B) Selected representative curves of individual kinetochore-to-pole distances from the cells shown in (A). Color shades are used to distinguish different tracks (t = 0 was set to anaphase onset).

(C) Comparison of the distribution of motion stages and velocity for the 240 s post-anaphase onset in untreated or Okadaic acid-treated HeLa cells is shown (3×GFP-CENP-A, 3×GFP-centrin; $n \geq 10$ each).

(D) Comparison of the proportion of anti-poleward motion during metaphase, untreated anaphase (n = 10), or Okadaic acid-treated (n = 18) anaphase HeLa cells is shown (3×GFP-CENP-A, 3×GFP-centrin).

(E) Kymographs as in (A) for cells expressing either wild-type Cyclin B or a non-degradable Cyclin B mutant. Arrowheads highlight spindle poles (green). Unpaired t tests were applied for comparison (****$p < 0.0001$ and **$p = 0.0031$; not significant, n.s.; C, $p = 0.235$; D, $p = 0.117$). SDs were measured across cells using the average behavior for kinetochores in each cell. Scale bars, 2 μm. See also Figure S3, Table S2, and Movie S3.

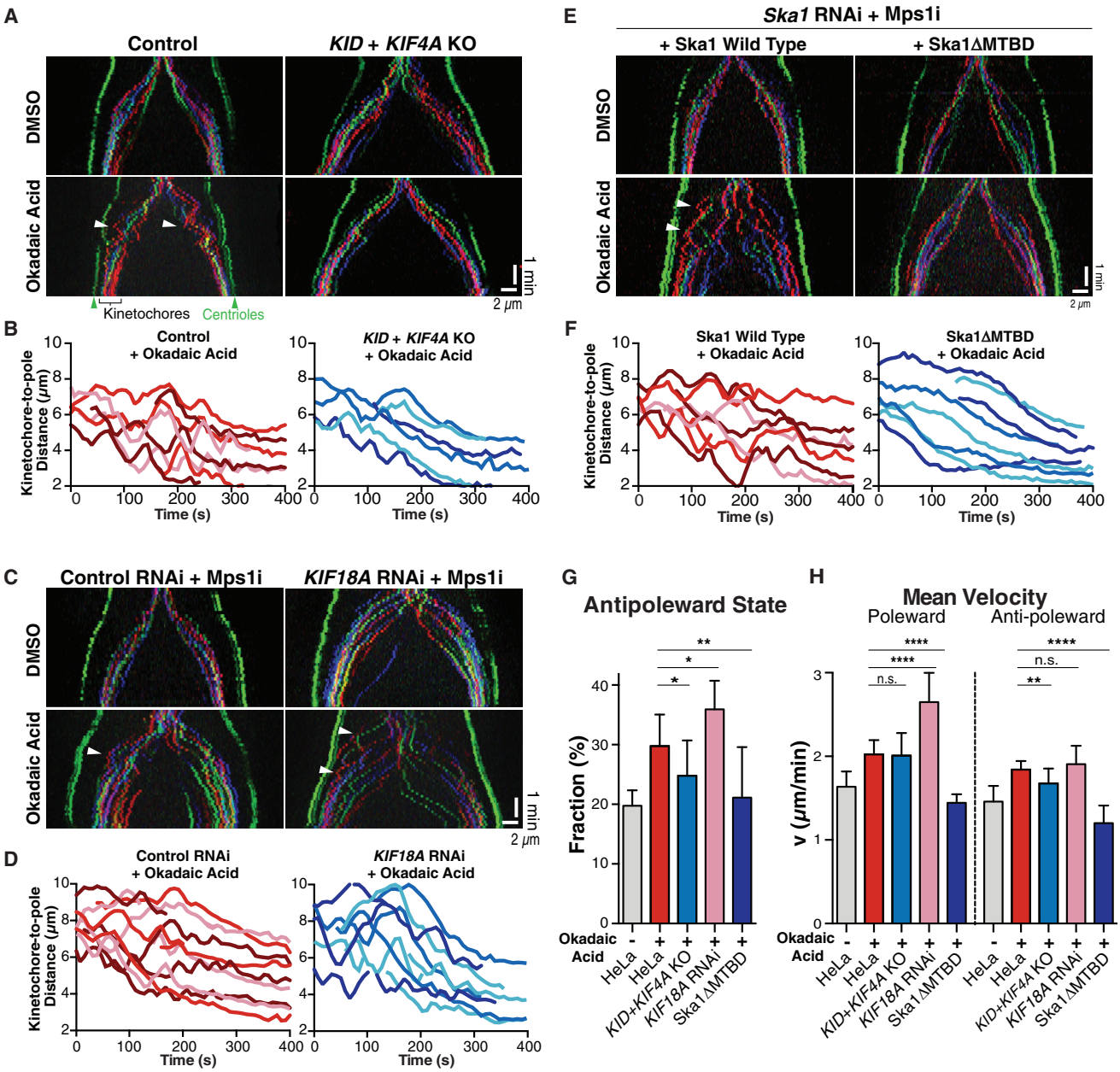

Figure 4. Chromosome and Kinetochore-Derived Forces Contribute to Anaphase Anti-poleward Motion in Okadaic Acid-Treated Cells

(A) Representative color-coded kymographs show HeLa cells (3×GFP-CENP-A, 3×GFP-centrin) undergoing anaphase either for control cells (left) or *KID* and *KIF4A* double-knockout cells (*KID* + *KIF4A* KO; right) treated with DMSO (upper panels; n = 10 or 6) or Okadaic acid (lower panels; n ≥ 10).

(B) Graph shows selected representative kinetochore-to-pole distances from (A).

(C) Kymographs as in (A) display cells treated with nontargeting control siRNAs (left) or *KIF18A* siRNA after 24 hr (right) incubated in DMSO (upper panels; n = 6 or 18) or Okadaic acid (lower panels; n = 6 or 5, respectively) and MPS1 inhibitor AZ3146.

(D) Graph shows selected representative kinetochore-to-pole distances from Okadaic acid-treated cells as displayed in (C).

(E) Kymographs as in (A) displaying cells in which either wild-type mCherry-Ska1 (left) or a Ska1ΔMTBD mutant (right) replaces endogenous Ska1(48 hr RNAi). Cells were treated with AZ3146 and DMSO (upper panels; n = 3 or 4) or AZ3146 and Okadaic acid (lower panels; n = 8 or 5, respectively).

(F) Graph shows selected representative kinetochore-to-pole distances from (E).

(G) Diagram displays the fraction of anti-poleward state of kinetochores 240 s post-anaphase onset for conditions (A)–(F). Unpaired t tests were performed to HeLa cells (n = 18): *KID* + *KIF4A* KO (n = 12), *p = 0.0225; *KIF18A* RNAi (n = 5), *p = 0.0285; Ska1ΔMTBD (n = 5), **p = 0.0096.

(H) Diagram displays the velocity of kinetochore motion 240 s post-anaphase onset for conditions (A)–(F). Unpaired t tests were performed for poleward motion to HeLa cells (n = 18): *KID* + *KIF4A* KO (n = 12), n.s., p = 0.854; *KIF18A* RNAi (n = 5), ****p < 0.0001; Ska1ΔMTBD (n = 5), ****p < 0.0001; and for anti-poleward motion: *KID* + *KIF4A* KO (n = 12), **p = 0.0033; *KIF18A* RNAi (n = 5), n.s., p = 0.3492; Ska1ΔMTBD (n = 5), ****p < 0.0001. Arrowheads highlight spindle poles (green) and examples of anti-poleward motion (white). Scale bars, 2 μm. See also Figure S4, Table S2, and Movie S4.

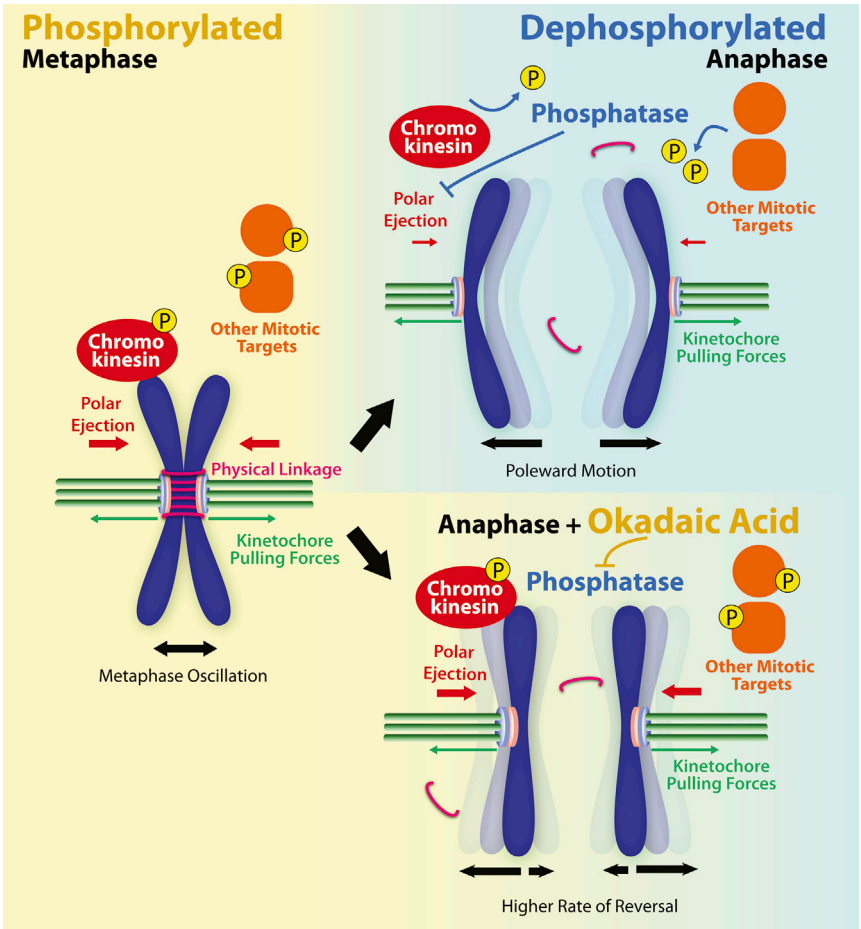

Figure 5. Model for the Regulatory Control of Chromosome Dynamics at the Metaphase-to-Anaphase Transition

In metaphase, chromosome oscillations are caused by chromokinesin-based polar ejection forces and kinetochore-derived forces. These activities are controlled by phosphorylation downstream of CDK1. At anaphase onset, CDK1 is inactivated and phosphatases reverse the phosphorylation of its substrates to downregulate polar ejection forces and kinetochore-derived forces that act through microtubule polymerization. This allows chromosomes to display net motion toward the spindle poles. In contrast, in the presence of the phosphatase inhibitor Okadaic acid, dephosphorylation is delayed such that chromokinesins and kinetochore-derived forces remain active. This maintains a metaphase-like oscillatory chromosome behavior in anaphase even after sister chromatid separation. Thus, mitosis is characterized by two distinct phases of chromosome motion, metaphase oscillations to align the chromosomes and poleward anaphase motion to segregate the chromosomes, and the switch in movement behavior is controlled by a regulatory transition.

(Tocris Bioscience) for 5 min or 10 μM STLC (Sigma) for 20 min (Figures 2E and 2F) or 2 hr (Figure S3C) before imaging. For RNAi, cells were transfected with 50 nM ON-TARGET plus small interfering RNAs (siRNAs) (Dharmacon) targeting *RAD21* (AUACCUUCUUGCAGACUGUUU), *KIF18A* (GCCAAUUCUUCGUAGUUUU), *Ska1* (pool targeting: GGACUUACUCGUUAUGUUA, UCAAUGGUGUUCCUUCGUA, UAUAGUGGAAGCUGACAUA, and CCGCUUAACCUAUAAUCAA), or a nontargeting control using Lipofectamine RNAi MAX (Invitrogen), following the manufacturer's instructions. Plasmids containing wild-type cyclin B1-mCherry or the non-degradable mutant (R42A and L45A) (Gavet and Pines, 2010; Vázquez-Novelle et al., 2014) were transfected into HeLa cells using FuGENE HD, according to the manufacturer's instructions, 24 hr prior to imaging.

Live-Cell Imaging

Cells were imaged in CO_2-independent media (Invitrogen) at 37°C. All images except laser microsurgery were acquired on a Nikon eclipse microscope equipped with a charge-coupled device (CCD) camera (Clara, Andor), using a 40× Plan Fluor objective 1.3 numerical aperture (NA) (Nikon) and appropriate fluorescence filters. Images of 3×GFP-CENP-A cell lines were acquired every 8 s using three (HeLa) or five (hTERT RPE-1 and Figure S3C) z sections at 0.7-μm intervals. Where indicated, cells were imaged at 4-s intervals using a single-plane focus. The mNeonGreen-PICH cells were imaged every 60 s at four z sections at 1-μm intervals. The laser microsurgery was conducted as described previously (Pereira et al., 2009), and it is detailed in the Supplemental Experimental Procedures. An extended description of the analysis of the time-lapse movies and kinetochore motion also is included in the Supplemental Experimental Procedures.

SUPPLEMENTAL INFORMATION

Supplemental Information includes Supplemental Experimental Procedures, four figures, two tables, four movies, and two data files and can be found with this article online at http://dx.doi.org/10.1016/j.celrep.2016.10.046.

AUTHOR CONTRIBUTIONS

Conceptualization, K.-C.S. and I.M.C.; Software, Z.B.; Formal Analysis, K.-C.S. and Z.B.; Investigation, K.-C.S. and N.S.; Data Curation, Z.B.; Writing – Original Draft, K.-C.S., Z.B., and I.M.C.; Writing – Review & Editing, N.S., H.M., and M.B.; Funding Acquisition & Supervision, H.M., M.B., and I.M.C.

ACKNOWLEDGMENTS

We thank António J. Pereira for assistance generating kymographs and members of the I.M.C. laboratory for their support, input, and helpful discussions. This work was supported by a Scholar award to I.M.C. from the Leukemia & Lymphoma Society, a grant from the NIH/National Institute of General Medical Sciences to I.M.C. (GM088313), a Research Scholar Grant to I.M.C. (121776) from the American Cancer Society, and a grant from the National Science Foundation (NSF) (PoLS PHY 1305537) to M.B. K.-C.S. was funded by FP7 Marie Curie Actions/Erwin Schrödinger Fellowship of the Austrian Science Fund (J-3478). H.M. is supported by the 7th framework program grant PRECISE from the European Research Council, FLAD Life Science 2020, and The Louis-Jeantet Foundation Young Investigator Award 2015.

Q1

Please cite this article in press as: Su et al., A Regulatory Switch Alters Chromosome Motions at the Metaphase-to-Anaphase Transition, Cell Reports (2016), http://dx.doi.org/10.1016/j.celrep.2016.10.046

Received: April 7, 2016
Revised: September 9, 2016
Accepted: October 13, 2016
Published: November 8, 2016

REFERENCES

Antonio, C., Ferby, I., Wilhelm, H., Jones, M., Karsenti, E., Nebreda, A.R., and Vernos, I. (2000). Xkid, a chromokinesin required for chromosome alignment on the metaphase plate. Cell *102*, 425–435.

Barisic, M., Aguiar, P., Geley, S., and Maiato, H. (2014). Kinetochore motors drive congression of peripheral polar chromosomes by overcoming random arm-ejection forces. Nat. Cell Biol. *16*, 1249–1256.

Burroughs, N.J., Harry, E.F., and McAinsh, A.D. (2015). Super-resolution kinetochore tracking reveals the mechanisms of human sister kinetochore directional switching. eLife *4*, e09500.

Canman, J.C., Cameron, L.A., Maddox, P.S., Straight, A., Tirnauer, J.S., Mitchison, T.J., Fang, G., Kapoor, T.M., and Salmon, E.D. (2003). Determining the position of the cell division plane. Nature *424*, 1074–1078.

Chan, K.L., North, P.S., and Hickson, I.D. (2007). BLM is required for faithful chromosome segregation and its localization defines a class of ultrafine anaphase bridges. EMBO J. *26*, 3397–3409.

Cheeseman, I.M., Niessen, S., Anderson, S., Hyndman, F., Yates, J.R., 3rd, Oegema, K., and Desai, A. (2004). A conserved protein network controls assembly of the outer kinetochore and its ability to sustain tension. Genes Dev. *18*, 2255–2268.

Civelekoglu-Scholey, G., He, B., Shen, M., Wan, X., Roscioli, E., Bowden, B., and Cimini, D. (2013). Dynamic bonds and polar ejection force distribution explain kinetochore oscillations in PtK1 cells. J. Cell Biol. *201*, 577–593.

Cong, L., Ran, F.A., Cox, D., Lin, S., Barretto, R., Habib, N., Hsu, P.D., Wu, X., Jiang, W., Marraffini, L.A., and Zhang, F. (2013). Multiplex genome engineering using CRISPR/Cas systems. Science *339*, 819–823.

Desai, A., Rybina, S., Müller-Reichert, T., Shevchenko, A., Shevchenko, A., Hyman, A., and Oegema, K. (2003). KNL-1 directs assembly of the microtubule-binding interface of the kinetochore in C. elegans. Genes Dev. *17*, 2421–2435.

Du, Y., English, C.A., and Ohi, R. (2010). The kinesin-8 Kif18A dampens microtubule plus-end dynamics. Curr. Biol. *20*, 374–380.

Dumont, S., Salmon, E.D., and Mitchison, T.J. (2012). Deformations within moving kinetochores reveal different sites of active and passive force generation. Science *337*, 355–358.

Funabiki, H., and Murray, A.W. (2000). The Xenopus chromokinesin Xkid is essential for metaphase chromosome alignment and must be degraded to allow anaphase chromosome movement. Cell *102*, 411–424.

Gavet, O., and Pines, J. (2010). Progressive activation of CyclinB1-Cdk1 coordinates entry to mitosis. Dev. Cell *18*, 533–543.

Häfner, J., Mayr, M.I., Möckel, M.M., and Mayer, T.U. (2014). Pre-anaphase chromosome oscillations are regulated by the antagonistic activities of Cdk1 and PP1 on Kif18A. Nat. Commun. *5*, 4397.

Hauf, S., Waizenegger, I.C., and Peters, J.M. (2001). Cohesin cleavage by separase required for anaphase and cytokinesis in human cells. Science *293*, 1320–1323.

Higuchi, T., and Uhlmann, F. (2005). Stabilization of microtubule dynamics at anaphase onset promotes chromosome segregation. Nature *433*, 171–176.

Inoué, S., and Salmon, E.D. (1995). Force generation by microtubule assembly/disassembly in mitosis and related movements. Mol. Biol. Cell *6*, 1619–1640.

Jaqaman, K., King, E.M., Amaro, A.C., Winter, J.R., Dorn, J.F., Elliott, H.L., McHedlishvili, N., McClelland, S.E., Porter, I.M., Posch, M., et al. (2010). Kinetochore alignment within the metaphase plate is regulated by centromere stiffness and microtubule depolymerases. J. Cell Biol. *188*, 665–679.

Joglekar, A.P., and Hunt, A.J. (2002). A simple, mechanistic model for directional instability during mitotic chromosome movements. Biophys. J. *83*, 42–58.

Levesque, A.A., and Compton, D.A. (2001). The chromokinesin Kid is necessary for chromosome arm orientation and oscillation, but not congression, on mitotic spindles. J. Cell Biol. *154*, 1135–1146.

Liu, Y., Nielsen, C.F., Yao, Q., and Hickson, I.D. (2014). The origins and processing of ultra fine anaphase DNA bridges. Curr. Opin. Genet. Dev. *26*, 1–5.

Maiato, H., and Lince-Faria, M. (2010). The perpetual movements of anaphase. Cell. Mol. Life Sci. *67*, 2251–2269.

Monnier, N., Barry, Z., Park, H.Y., Su, K.C., Katz, Z., English, B.P., Dey, A., Pan, K., Cheeseman, I.M., Singer, R.H., and Bathe, M. (2015). Inferring transient particle transport dynamics in live cells. Nat. Methods *12*, 838–840.

Ohsugi, M., Tokai-Nishizumi, N., Shiroguchi, K., Toyoshima, Y.Y., Inoue, J., and Yamamoto, T. (2003). Cdc2-mediated phosphorylation of Kid controls its distribution to spindle and chromosomes. EMBO J. *22*, 2091–2103.

Oliveira, R.A., Hamilton, R.S., Pauli, A., Davis, I., and Nasmyth, K. (2010). Cohesin cleavage and Cdk inhibition trigger formation of daughter nuclei. Nat. Cell Biol. *12*, 185–192.

Parry, D.H., Hickson, G.R., and O'Farrell, P.H. (2003). Cyclin B destruction triggers changes in kinetochore behavior essential for successful anaphase. Curr. Biol. *13*, 647–653.

Pereira, A.J., Matos, I., Lince-Faria, M., and Maiato, H. (2009). Dissecting mitosis with laser microsurgery and RNAi in Drosophila cells. Methods Mol. Biol. *545*, 145–164.

Rieder, C.L., Davison, E.A., Jensen, L.C., Cassimeris, L., and Salmon, E.D. (1986). Oscillatory movements of monooriented chromosomes and their position relative to the spindle pole result from the ejection properties of the aster and half-spindle. J. Cell Biol. *103*, 581–591.

Schmidt, J.C., Arthanari, H., Boeszoermenyi, A., Dashkevich, N.M., Wilson-Kubalek, E.M., Monnier, N., Markus, M., Oberer, M., Milligan, R.A., Bathe, M., et al. (2012). The kinetochore-bound Ska1 complex tracks depolymerizing microtubules and binds to curved protofilaments. Dev. Cell *23*, 968–980.

Skibbens, R.V., Skeen, V.P., and Salmon, E.D. (1993). Directional instability of kinetochore motility during chromosome congression and segregation in mitotic newt lung cells: a push-pull mechanism. J. Cell Biol. *122*, 859–875.

Skibbens, R.V., Rieder, C.L., and Salmon, E.D. (1995). Kinetochore motility after severing between sister centromeres using laser microsurgery: evidence that kinetochore directional instability and position is regulated by tension. J. Cell Sci. *108*, 2537–2548.

Stumpff, J., von Dassow, G., Wagenbach, M., Asbury, C., and Wordeman, L. (2008). The kinesin-8 motor Kif18A suppresses kinetochore movements to control mitotic chromosome alignment. Dev. Cell *14*, 252–262.

Stumpff, J., Wagenbach, M., Franck, A., Asbury, C.L., and Wordeman, L. (2012). Kif18A and chromokinesins confine centromere movements via microtubule growth suppression and spatial control of kinetochore tension. Dev. Cell *22*, 1017–1029.

Vázquez-Novelle, M.D., Sansregret, L., Dick, A.E., Smith, C.A., McAinsh, A.D., Gerlich, D.W., and Petronczki, M. (2014). Cdk1 inactivation terminates mitotic checkpoint surveillance and stabilizes kinetochore attachments in anaphase. Curr. Biol. *24*, 638–645.

Vladimirou, E., Harry, E., Burroughs, N., and McAinsh, A.D. (2011). Springs, clutches and motors: driving forward kinetochore mechanism by modelling. Chromosome Res. *19*, 409–421.

Wan, X., Cimini, D., Cameron, L.A., and Salmon, E.D. (2012). The coupling between sister kinetochore directional instability and oscillations in centromere stretch in metaphase PtK1 cells. Mol. Biol. Cell *23*, 1035–1046.

Wandke, C., Barisic, M., Sigl, R., Rauch, V., Wolf, F., Amaro, A.C., Tan, C.H., Pereira, A.J., Kutay, U., Maiato, H., et al. (2012). Human chromokinesins

promote chromosome congression and spindle microtubule dynamics during mitosis. J. Cell Biol. *198*, 847–863.

Wang, L.H., Schwarzbraun, T., Speicher, M.R., and Nigg, E.A. (2008). Persistence of DNA threads in human anaphase cells suggests late completion of sister chromatid decatenation. Chromosoma *117*, 123–135.

Wurzenberger, C., and Gerlich, D.W. (2011). Phosphatases: providing safe passage through mitotic exit. Nat. Rev. Mol. Cell Biol. *12*, 469–482.

Wurzenberger, C., Held, M., Lampson, M.A., Poser, I., Hyman, A.A., and Gerlich, D.W. (2012). Sds22 and Repo-Man stabilize chromosome segregation by counteracting Aurora B on anaphase kinetochores. J. Cell Biol. *198*, 173–183.

Zhai, Y., Kronebusch, P.J., and Borisy, G.G. (1995). Kinetochore microtubule dynamics and the metaphase-anaphase transition. J. Cell Biol. *131*, 721–734.

Cell Reports, Volume *17*

Supplemental Information

A Regulatory Switch Alters Chromosome Motions at the Metaphase-to-Anaphase Transition

Kuan-Chung Su, Zachary Barry, Nina Schweizer, Helder Maiato, Mark Bathe, and Iain McPherson Cheeseman

Supplemental Figures and Legends

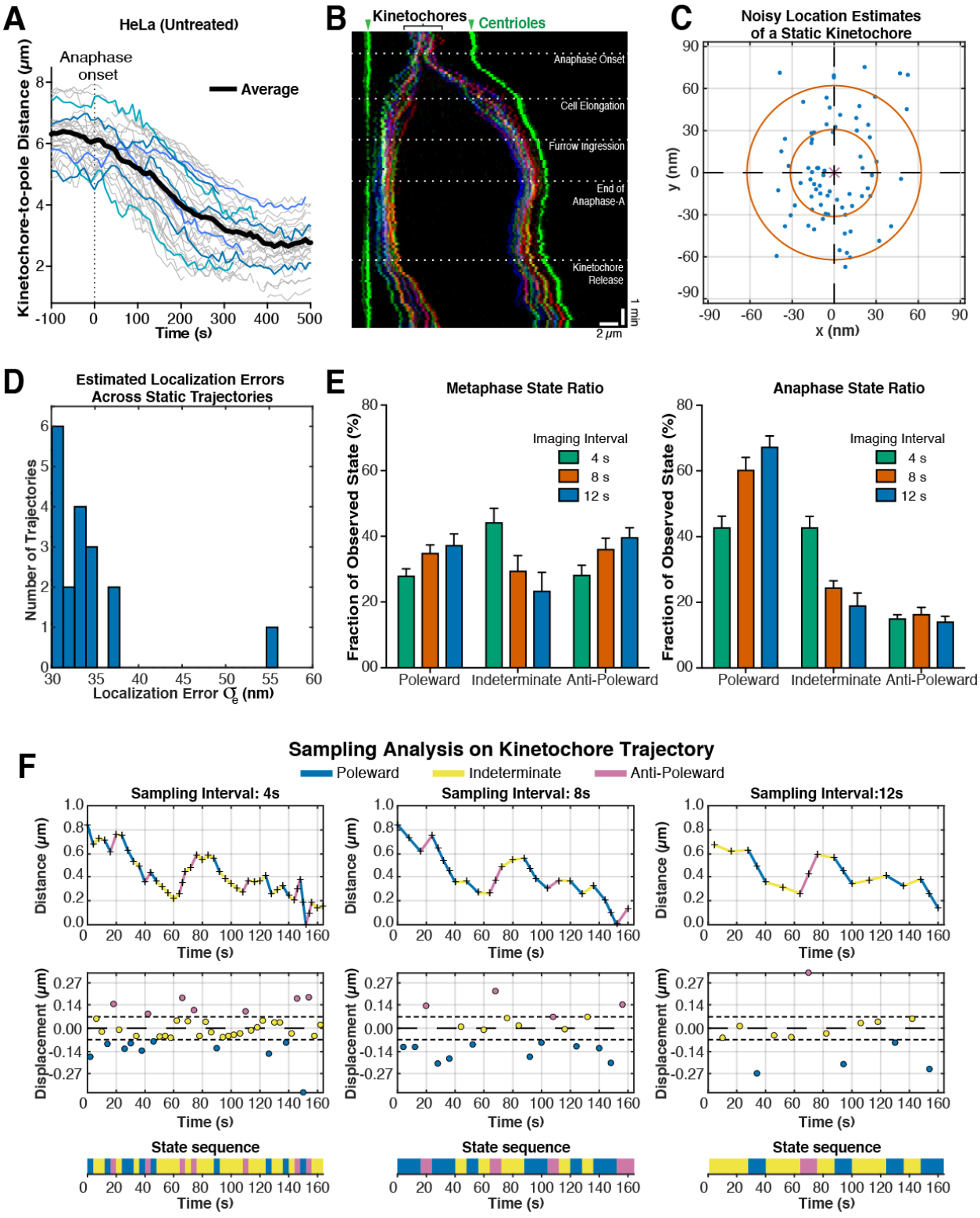

Figure S1. Characterization of anaphase chromosome dynamics from single-particle tracking and trajectory analysis. Related to Figure 1. (A) Kinetochore-to-pole distances for an example untreated HeLa cell. Representative distance trajectories over time are labeled in blue. The average distance measured over all trajectories in this cell over time is depicted by the bold black line. Anaphase onset is labeled as t = 0. (B) Color-coded kymograph of the time-lapse movie corresponding to Figure 1D aligned to one pole. The dashed lines indicate distinct anaphase events from sister chromatid separation onwards. (C) Example serial localizations from a single kinetochore tracked in a fixed HeLa cell (solid blue dots) plotted together with the mean position of the kinetochore (magenta 'x') determined from the average of the serial kinetochore localizations. Red circles denote successive standard deviations from the mean measured by a normal distribution fitted to the localizations. The estimated localization error for this single kinetochore corresponds to the standard deviation. (D) Histogram of localization errors estimated from multiple kinetochores as depicted in Figure S1C. The localization error determined from this fixed cell (n = 18 kinetochores) was 34.2 ± 5.8 nm (mean ± s.d.). (E) State ratio comparison of untreated HeLa cells during metaphase (left) or anaphase (right) imaged at 4 second intervals and subsequently coarsened to 8 and 12 second intervals by omitting successive time-frames (n=8 cells). (F) Example kinetochore distance trajectory in anaphase imaged at 4 seconds/frame. Top: relative distance of the kinetochore from its spindle pole over the entire observed trajectory. Each curve is annotated using colors that denote the state of motion of the kinetochore during the corresponding interval. Middle: displacements (change in distance between successive time points) along the distance trajectory. The top and bottom dotted lines denote the localization error threshold that determines whether kinetochore motion is classified as poleward/anti-poleward or indeterminate. A positive displacement represents an anti-poleward motion in this regime (an increase in distance from the spindle pole). Bottom: the state sequence, or series of annotations of poleward/anti-poleward/indeterminate kinetochore motions, at successive time points in the trajectory. From left to right, the temporal sampling of the original trajectory is "coarsened" computationally from the original experimental imaging time sampling of 4 seconds/frame to 8 and 12 seconds/frame to test the role of temporal sampling on motion classification.

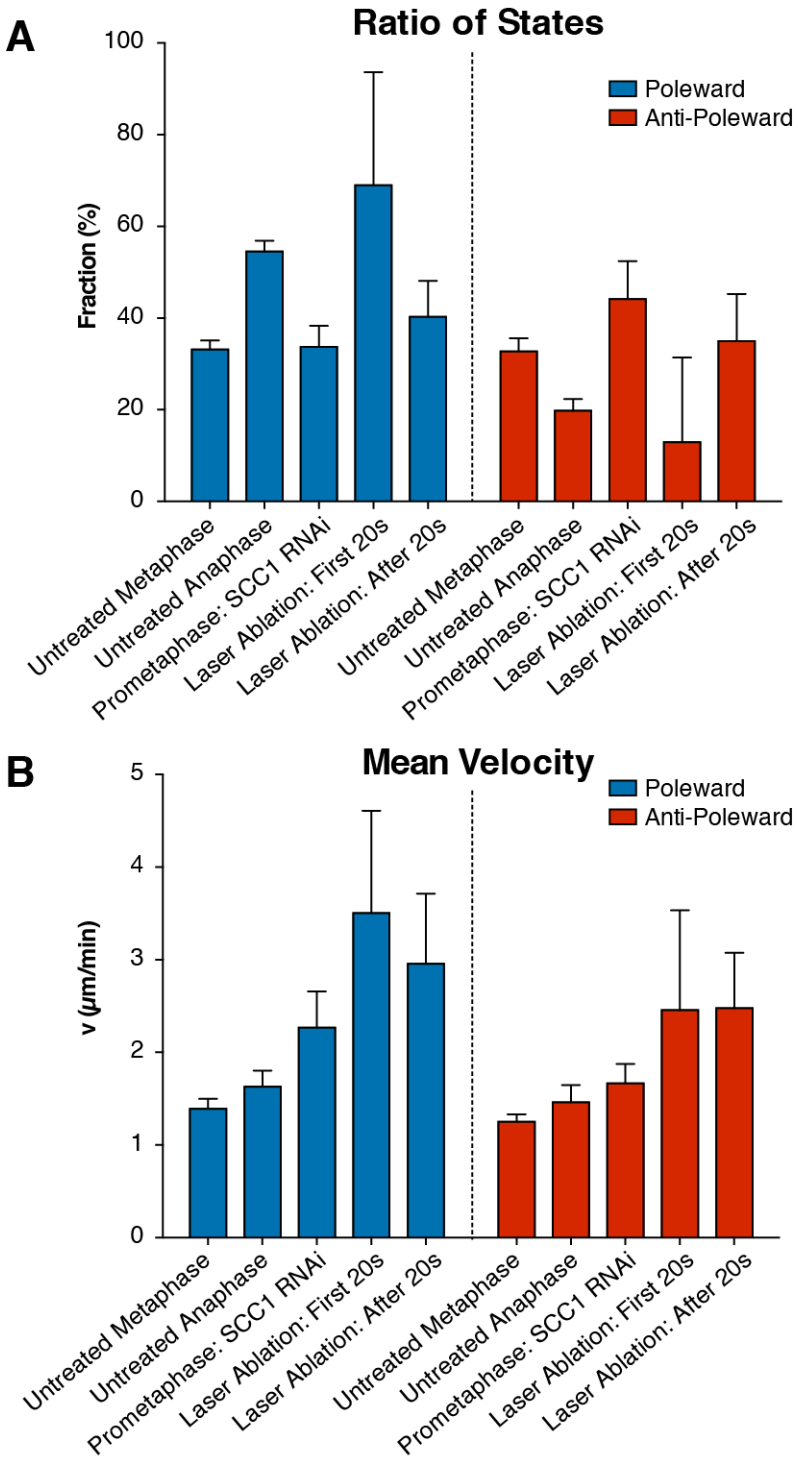

Figure S2. Effects of removal of physical connections between sister chromatids on chromosome dynamics. Related to Figure 4. Comparison of distribution of kinetochore motion stages (A) and velocity (B) during in HeLa cells (3xGFP-CENP-A, 3xGFP-centrin) during untreated Metaphase or Anaphase (n=10 each), after cohesin subunit SCC1 RNAi (n=13) or Laser ablation (n=29).

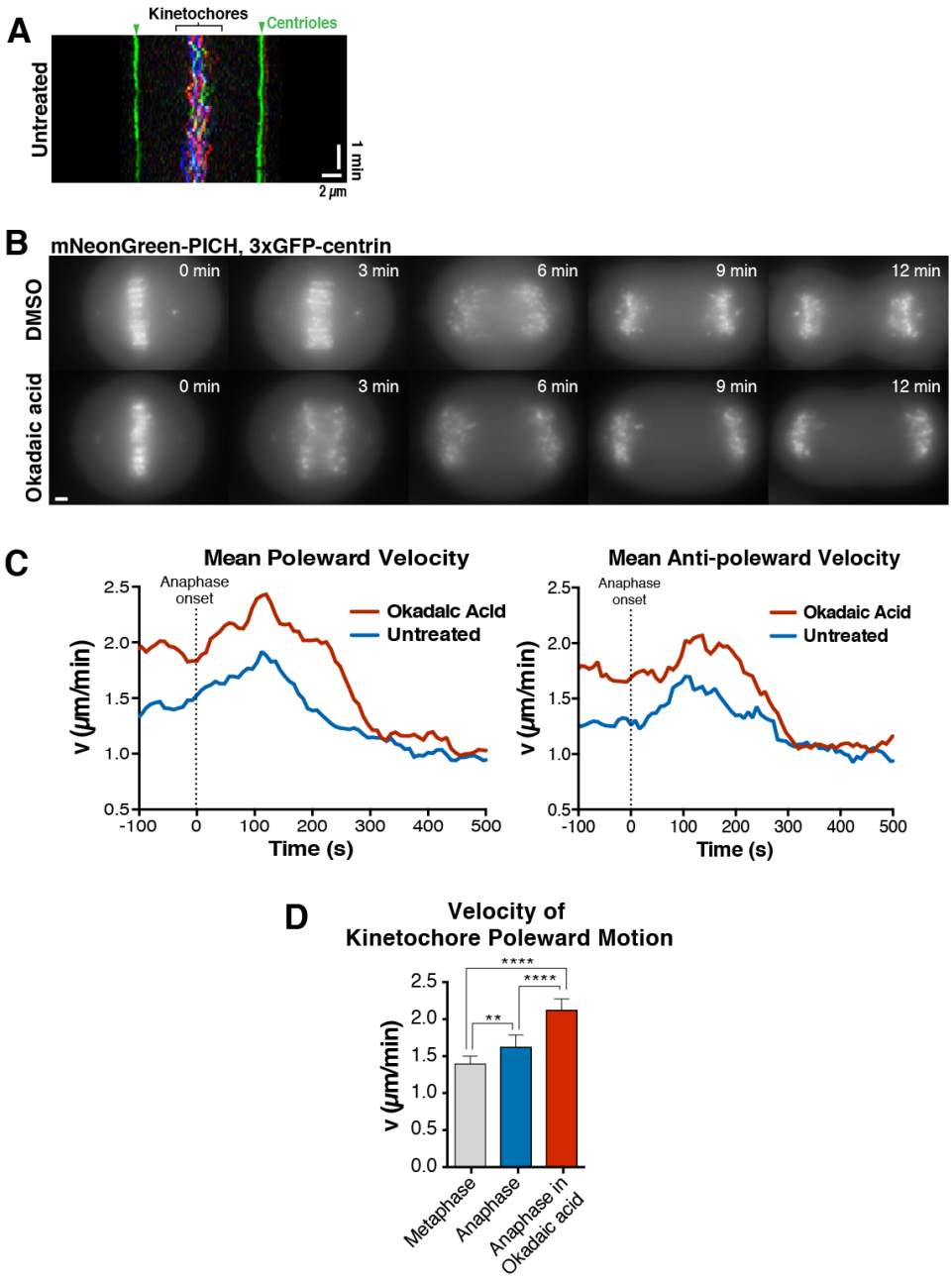

Figure S3. Effects of Okadaic acid on anaphase cell behavior and comparison to metaphase. Related to Figure 3. (A) Color-coded metaphase kymograph of an untreated (left n=10) HeLa cell (3xGFP-CENP-A, 3xGFP-centrin). (B) Representative time-lapse stills (maximal intensity projections) of HeLa cells expressing mNeonGreen-PICH, 3xGFP-centrin entering anaphase in presence of DMSO (upper row, n=10) or Okadaic acid (lower row, n=8). (C) Graphs showing distribution of motion stages, the average poleward velocity (left) or anti-poleward velocity (right) in untreated HeLa cells or Okadaic acid treated HeLa cells (3xGFP-CENP-A, 3xGFP-centrin) over time (n=10 cells each). (D) Comparison of distribution of anti-poleward motion in metaphase cells, untreated anaphase, or Okadaic acid-treated anaphase HeLa cells (3xGFP-CENP-A, 3xGFP-centrin; n>10 each; Unpaired t test results: **** $p<0.0001$, ** $p=0.0017$). Scale bars, 2μm.

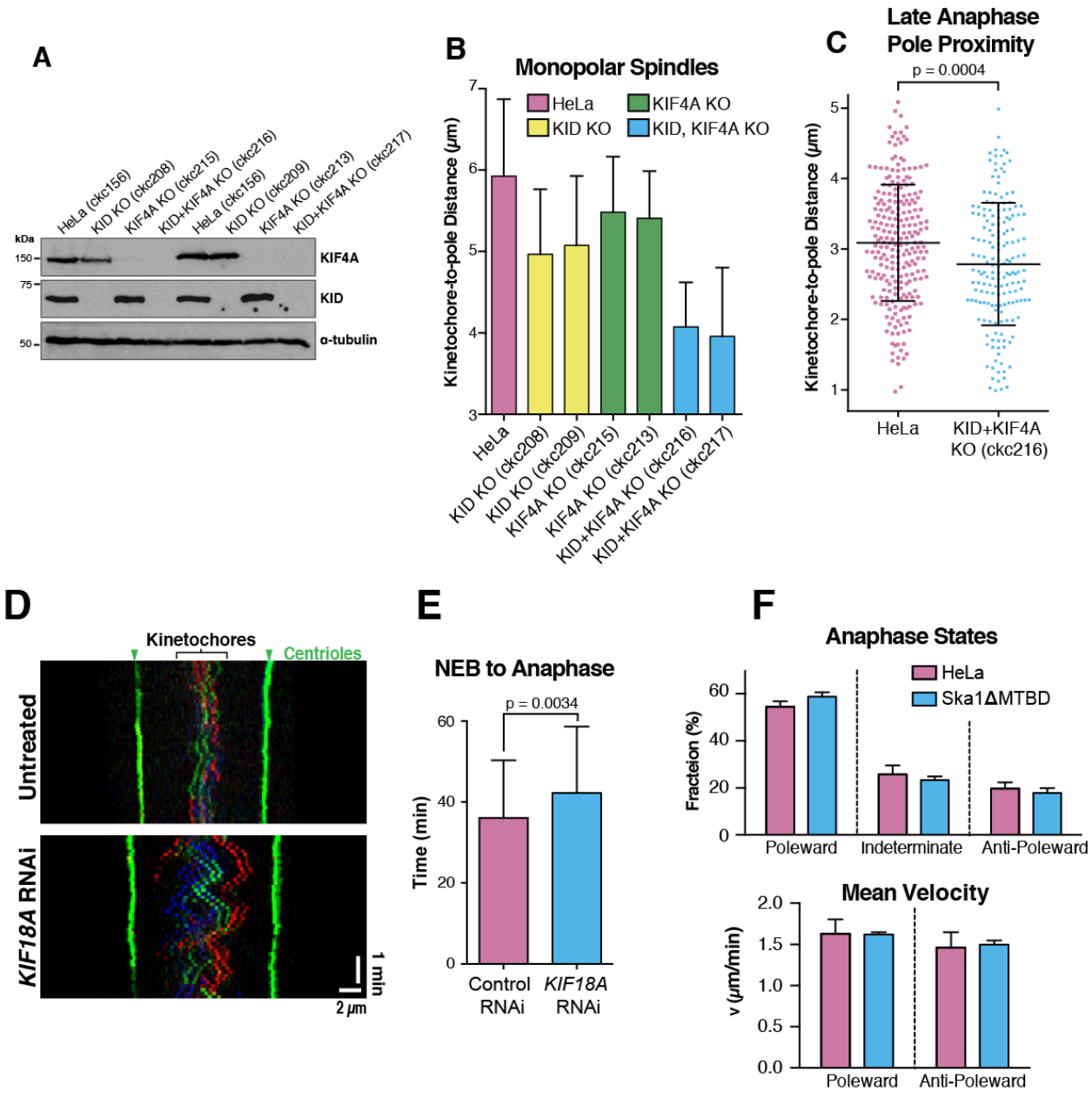

Figure S4. Characterization of Cell lines and Perturbations. Related to Figure 4. (A) Western blots probed for KIF4A, KID and *α*-tubulin (as a loading control) for HeLa cells (3xGFP-CENP-A, 3xGFP-centrin) in which the chromokinesins KID and/or KIF4A were eliminated using CRISPR/Cas9-mediated gene editing approaches. Asterisks indicate cells lines used in this study. (B) Kinetochore to pole distance in STLC treated cells with monopolar spindles (n>20 cells each). 2 independent single and double knock out cell lines of KID, KIF4A were compared to their progenitor HeLa cell line (3xGFP-CENP-A, 3xGFP-centrin). Error bar indicate standard deviation (C) Distribution of kinetochore to pole distance between control cells and KID, KIF4A double knock out HeLa cells (3xGFP-CENP-A, 3xGFP-centrin) 6 minutes after anaphase onset (n>174 kinetochores each pooled from 7 cells). Lines indicate average and standard deviation. P indicates

unpaired t test result. (D) Representative color-coded metaphase kymograph of an untreated (n=10) HeLa cell (3xGFP-CENP-A, 3xGFP-centrin) or treated with siRNA against KIF18A after 48h (right n=20). (E) Average nuclear envelope breakdown (NEB) to anaphase duration of cells after Control (n=104) or KIF18A (n=114) RNAi. P indicates unpaired t test result. (F) Comparison of relative ratio of states and velocity between untreated HeLa cells (n=10) and cells expressing Ska1-dMT mutant (n=5) after depletion of the endogenous protein.

Supplemental Movie Legends

Movie 1. **Anaphase chromosome dynamics in human cells.** Related to Figure 1. (Left) Untreated HeLa and hTERT RPE-1 cells (both expressing 3xGFP-CENP-A, 3xGFP-centrin) undergoing anaphase. t=0 was set to anaphase onset, 8 s intervals. (Right) Untreated HeLa cell (3xGFP-CENP-A, 3xGFP-centrin) imaged from metaphase to kinetochore release (with the stages indicated). t=0 was set to anaphase onset, 10 s intervals.

Movie 2. **Physical connections between sister chromatids are not required for anti-poleward motion.** Related to Figure 2. HeLa cell (3xGFP-CENP-A, 3xGFP-centrin) after cohesin (RAD21) depletion (upper left) at 8 s intervals, after kinetochore laser ablation (upper right) at 5 s intervals, displaying monopolar spindles induced by STLC treatment alone (bottom left) or additionally treated with MPS1i (bottom right) at 8s intervals. Boxes indicate tracked centrioles (green) or kinetochores displayed in figure graph. t=0 was set to beginning of movie.

Movie 3. **Perturbing the cellular phosphorylation state induces anaphase anti-poleward chromosome motion.** Related to Figure 3. HeLa cells (3xGFP-CENP-A, 3xGFP-centrin) untreated (upper left), in Okadaic acid (bottom left), expressing wild type (upper right) or non-degradable (bottom right) Cyclin B. t=0 was set to anaphase onset, 8 s intervals.

Movie 4. **Chromosome and kinetochore-derived forces contribute to anaphase anti-poleward motion in Okadaic acid-treated cells.** Related to Figure 4. HeLa cells (3xGFP-CENP-A, 3xGFP-centrin) either untreated, after KIF18A RNAi (+MPS1i), in the KID+KIF4A knockout, or following Ska1 replacement with a Ska1 ΔMTBD mutant (+MPS1i) treated with DMSO or Okadaic acid. t=0 was set to anaphase onset, 8 s intervals.

Table S1. Parameters of Anaphase Spindle and Kinetochore Motion. Related to Figure 1.

Cell Type	Anaphase Spindle Length		Maximum Pole Separation Speed	
	Early	Late	Velocity	Reached at Time After Anaphase Onset
HeLa	~12 µm	~20 µm	2.7 ± 0.6 µm/min	~1 min
hTERT-RPE1	~12 µm	~19 µm	2.6 ± 0.6 µm/min	~1.3 min

Cell Type	Anaphase Kinetochore to Pole Distance		Averaged Maximum Kinetochore to Pole Motion	
	Early	Late	Velocity	Reached at Time After Anaphase Onset
HeLa	6.13 ± 0.2 µm	3.2 ± 0.3 µm	1.17 ± 0.2 µm/min	~2 min
hTERT-RPE1	5.9 ± 0.6 µm	3.1 ± 0.6 µm	2.04 ± 0.7 µm/min	~0.66min

Cell Type	Early Anaphase (240s HeLa, 152s hTERT-RPE1)				
	Poleward State	Average Poleward Motion Speed	Pause State	Anti-poleward State	Average Anti-poleward Motion Speed
HeLa	54.5±2.4%	1.63±0.17 µm/min	25.8±3.8%	19.8±2.6%	1.46±0.19 µm/min
hTERT-RPE1	62.6±4.2%	2.03±0.16 µm/min	17.7±2.5%	19.7±3.6%	1.76±0.20 µm/min

Table S2. Kinetochore Dynamics of HeLa Cells. Related to Figure 1-4.

Condition (Number of Cells)	Frequency of State (%)			Velocity (µm/min)	
	Poleward	Indeterminate	Anti-poleward	Poleward	Anti-poleward
Untreated Metaphase (10)	33.1±2.0	34.2±2.9	32.7±2.9	1.39±0.11	1.25±0.08
Untreated Anaphase (10)	54.5±2.4	25.8±3.8	19.8±2.6	1.63±0.17	1.46±0.19
Prometaphase: *RAD21* RNAi (13)	33.7±4.6	22.2±6.5	44.1±8.3	2.27±0.39	1.66±0.21
Laser Ablation: First 20s (29)	69.0±24.7	18.1±21.0	12.9±18.4	3.50±1.11	2.45±1.08
Laser Ablation: After 20s (29)	40.3±7.8	24.7±9.1	35.0±10.3	2.96±0.76	2.48±0.60
Anaphase in Okadaic Acid (18)	52.6±4.4	17.6±2.1	29.8±5.3	2.04±0.18	1.84±0.10
Anaphase of *KID+KIF4A* KO in Okadaic Acid (12)	57.0±5.4	18.1±3.5	24.8±5.9	2.01±0.27	1.68±0.18
Anaphase of *KIF18A* RNAi in Okadaic Acid (5)	49.5±3.5	14.5±2.6	35.9±4.8	2.62±0.31	1.91±0.22
Anaphase of SKA1-ΔMTBD in Okadaic Acid (5)	46.4±8.6	32.4±7.1	21.1±8.5	1.54±0.24	1.20±0.21
Untreated Anaphase of SKA1- ΔMTBD (5)	58.8±1.9	23.4±1.5	17.9±2.0	1.62±0.03	1.50±0.05

Supplemental Datasets

Velocity distributions. Related to Figure 1, 3 and 4. Cell-to-cell heterogeneity of measured velocities for indicated conditions and total number steps of displacement displayed. Shown are the distributions of instantaneous poleward (positive values) and anti-poleward velocities (negative values) for every anaphase frame within the window used for calculations of all trajectories within a particular cell as determined from the trajectory annotations and displacements. Orange lines and label indicate average value and standard deviation.

TrackFiles.ZIP. Related to Figure 1-4**.** Document containing all .mdf files of every cell tracked in this study.

Supplemental Experimental Procedures

Cell Lines Used in This Study

ckc156: HeLa - 3xGFP-CENP-A, 3xGFP-centrin

ckc094: hTERT RPE-1 - 3xGFP-CENP-A, 3xGFP-centrin

ckc152: HeLa - mNeonGreen-PICH, 3xGFP-centrin

ckc208: HeLa3xGFP-CENP-A - 3xGFP-centrin, *KID* knockout

ckc209: HeLa3xGFP-CENP-A - 3xGFP-centrin, *KID* knockout

ckc213: HeLa3xGFP-CENP-A - 3xGFP-centrin, *KIF4A* knockout

ckc215: HeLa3xGFP-CENP-A - 3xGFP-centrin, *KIF4A* knockout

ckc216: HeLa3xGFP-CENP-A - 3xGFP-centrin, *KID* knockout, *KIF4A* knockout

ckc217: HeLa3xGFP-CENP-A - 3xGFP-centrin, *KID* knockout, *KIF4A* knockout

ckc101: HeLa3xGFP-CENP-A - 3xGFP-centrin, mCherry-Ska1-WT (hardened)

ckc103: HeLa3xGFP-CENP-A - 3xGFP-centrin, mCherry-Ska1-ΔMTBD (hardened)

Laser microsurgery

Single kinetochores were ablated by eight consecutive pulses (10 Hz repetition rate; pulse width: 8-10 ns; pulse energy: 1.5-2 μJ) derived from a doubled-frequency Elforlight laser (FQ-500-532) mounted on an inverted microscope (TE2000U; Nikon) equipped with a CSU-X1 spinning-disk confocal head (Yokogawa Corporation of America). Cells were imaged using a 100x 1.4 NA Plan-Apochromatic differential interference contrast objective (Nikon). Images were detected with an iXonEM+ EM-CCD camera (Andor Technology), using the NIS-Elements software (Nikon Instruments Inc.).

Image processing

Time-lapse images of 3xGFP-CENP-A cell lines were background subtracted (rolling ball radius: 2 pixels), sum projected and brightness/contrast adjusted in ImageJ/Fiji before further processing or analysis. Generation of kymographs was performed as described previously (Pereira and Maiato, 2010). Briefly, guided-kymographs were generated after manual spindle pole tracking, the coordinates of which were used to compensate for spindle rotation and translation over time, thereby stabilizing a virtual equator in the horizontal center of the kymograph. To collapse the kymograph, a routine was used that assigns an RGB color gradient to the vertical axis of each kymograph frame.

Analysis of kinetochore motion

All computational analyses of particle trajectories and the downstream analysis of kinetochore motion were performed using MATLAB 2014a. Single-particle trajectories (SPTs) of kinetochore motion were generated from sequential spatial localizations using the MTrackJ software package (Meijering, 2006) provided in Fiji/ImageJ. Individual kinetochore localizations were obtained manually using centroid fitting with a 9x9 pixel grid. Care was taken to avoid invalid assignments in which one kinetochore trajectory was connected with an unrelated kinetochore trajectory. With this in mind, merging and splitting events (two objects overlapping/separating), as well as gap closing connecting objects that disappear and reappear in a later frame (Jaqaman et al., 2008) were forbidden to eliminate the chances of these occurrences. In cases where there was

uncertainty in sequential particle localizations between two frames, trajectories were terminated.

To determine the localization error associated with estimated kinetochore positions, HeLa cells were fixed (10 min in 4% formaldehyde) and static kinetochores were imaged using the same imaging protocol that was applied to live cells. Kinetochores were tracked using the same parameters in MTrackJ (centroid fitting) to generate time-series single particle trajectories of stationary kinetochores. Motions of individual points along each trajectory were assumed to be due solely to independent localization errors, excluding stage drift and thermal motion. Under this assumption, the spatial localizations of individual particles can be modeled as distributed according to a Gaussian with the mean centered on the true (fixed) particle position and a standard deviation that is equal to the localization error. Figure S1C shows the localization error and fitting procedure for a single example kinetochore, where σ_e is the localization error associated with the normal distribution fit to the sequential localization measurements. Analyses of eighteen such trajectories of stationary kinetochores were performed with their localization errors individually computed in this manner (Figure S1D). The overall distribution from compiling the individual localization errors for each trajectory estimated in this manner was then used to obtain the final mean-value estimate of the localization error that was subsequently used for classification of kinetochore motion behaviors (34.2 ± 5.8 nm; mean ± s.d.). Kinetochores and spindle poles were assumed to have equal localization errors.

To classify poleward and anti-poleward moving kinetochores (Figure S1F), we analyzed the single-step-level dynamics of individual kinetochore trajectories.

Kinetochore trajectories were assigned to their corresponding spindle poles based on the minimum mean distance during anaphase. In KIF18A-depleted cells, chromosomes do not align to form a proper metaphase plate, so the assignment of the corresponding spindle pole was based on the minimum distance of the last tracked frame for the kinetochore in question. The time of anaphase onset for each individual cell was defined as the time point immediately prior to the separation of sister chromatid populations as annotated manually using visual inspection based on the distance between the kinetochore-spindle pole groups. For anaphase motion, we analyzed the first 240 seconds in HeLa cells or 152 seconds in hTERT-RPE1 cells after anaphase onset. For metaphase, we analyzed motions of the first 320 seconds of a >600 second movie in which the cell remained in metaphase throughout the imaging process.

After the assignment of kinetochores to spindle poles, the change in distance (displacement) between each kinetochore and their corresponding spindle poles was computed over time. Measurements of these displacements will be slight underestimates due to the possibility of out-of-plane motion that is lost in projection of kinetochore and spindle pole positions to the imaging plane. Displacements were then analyzed to determine whether a kinetochore was moving poleward or anti-poleward. Note that to classify poleward/anti-poleward motion based on the change in distance between the kinetochore in question and its assigned spindle pole, the uncertainty in the distance, σ_D, between the two objects rather than simply the localization error, σ_e, of each object itself must be considered. This distance uncertainty is derived from the propagation of error in computing the distance from the localizations of the kinetochores and spindle poles, where the uncertainty in the distance is related to the localization

error by $\sigma_D = \sqrt{2}\sigma_e$. An event was defined as "indeterminate" if the kinetochore displacement (Δx) between two time points was smaller than $\sqrt{2}\sigma_D$. Adjusting this ad hoc threshold results in a trade-off between the detectability of kinetochore poleward/anti-poleward motions and the mis-assignment of localization noise to these motion states in the analysis.

Cell-to-cell heterogeneity in kinetochore displacement as well as velocity distributions were characterized following annotation of trajectories into poleward and anti-poleward states. Additionally, the percentage of time spent in each state across all kinetochores for each individual cell was computed over the anaphase period. The sample mean of each metric for each cell was used to compute the overall distribution of the metric for each condition or cell line. For the calculation of statistical significance between treatment conditions or perturbations, Prism 6 (GraphPad) was used to perform unpaired, two-tailed Student's t-tests. Independent samples tested represent measurements from distinct cells in a given condition, with the set of individual trajectories per cell contributing to the mean behavior for that cell. At least five independent samples were analyzed in each case. To highlight this point, distributions of both poleward and anti-poleward velocities were plotted for each cell and are consistent within their groups. The cell-by-cell distributions of velocities for cells analyzed in Figures 1, 3 and 4 can be found in the Supplemental Dataset along with the complete data set from our tracking of each individual cell and condition as both MATLAB .mat data files as well as MTrackJ .mdf trajectory files.

We additionally evaluated the sensitivity of classified kinetochore behaviors to imaging frame rate, including the classification of poleward versus anti-poleward motion

and their associated state lifetimes. For this analysis, untreated HeLa cell kinetochore trajectories obtained using 4 seconds/frame imaging conditions were “coarsened” computationally to decrease sampling to 8 and then 12 seconds/frame by omitting data from neighboring time-points. Results indicate that trajectory coarsening results in an overall increase in displacement magnitude between successive frames, as expected for a random process with drift (Figure S1F; Berg, 1993; Monnier et al., 2015; Monnier et al., 2012). Accordingly, a smaller fraction of kinetochore displacements is classified as “indeterminate” (Figure S1E) because more displacements per trajectory exceed the localization error threshold. Associated estimations of the lifetimes of individual motion states are also observed to depend strongly on sampling frequency because of the similar dependence of active versus diffusive transport on the time-scale of observation. Thus, the local lifetime of a given poleward/anti-poleward processive motion depended strongly on sampling frequency, and was omitted from analysis.

An example “coarsened” (4s, 8s, 12 s/frame) trajectory is shown in Figure S1F. This trajectory is annotated in color using its “state sequence” corresponding to the intervals that the algorithm has classified as poleward, anti-poleward, or indeterminate. At 4 s/frame, a large fraction of the intervals annotated fall below the minimum threshold for labeling a particular displacement as poleward or anti-poleward. This is due to the average step size that the kinetochore moves during the 4 second interval falling near or below the detection threshold that is imposed by the localization error. Decreasing temporal resolution (4 s/frame to 8 s/frame) results in larger displacements, leading to more intervals that are positively annotated as having motion beyond the noise threshold. Trajectories can be coarsened further (8 s/frame to 12 s/frame) at the cost of

decreased temporal resolution, which may result in the failure to detect motion dynamics on faster timescales. Given this sensitive dependence of motion state lifetimes on sampling frame rate, we refrained from reporting motion state lifetime information.

Supplemental References

Berg, H. (1993). Random Walks in Biology Princeton University Press. Princeton, NJ, 30.

Jaqaman, K., Loerke, D., Mettlen, M., Kuwata, H., Grinstein, S., Schmid, S.L., and Danuser, G. (2008). Robust single-particle tracking in live-cell time-lapse sequences. Nature methods *5*, 695-702.

Meijering, E. (2006). MTrackJ: A Java program for manual object tracking. University Medical Center Rotterdam,[Online] Available: http://wwwimagescienceorg/meijering/software/mtrackj.

Monnier, N., Barry, Z., Park, H.Y., Su, K.C., Katz, Z., English, B.P., Dey, A., Pan, K., Cheeseman, I.M., Singer, R.H.*, et al.* (2015). Inferring transient particle transport dynamics in live cells. Nature methods *12*, 838-840.

Monnier, N., Guo, S.M., Mori, M., He, J., Lenart, P., and Bathe, M. (2012). Bayesian approach to MSD-based analysis of particle motion in live cells. Biophys J *103*, 616-626.

Pereira, A.J., and Maiato, H. (2010). Improved kymography tools and its applications to mitosis. Methods *51*, 214-219.